Acta Manilana 63 (2015), pp. 7–15
Printed in the Philippines
ISSN: 0065–1370

Synthesis and characterization of graphene-supported Pd/Ni/Sn electrocatalyst for direct ethanol fuel cells

Jan Rotsen Kyle A. Delos Santos[1], Arvee M. De Jesus[2], Joshua L. Tan[3], & Bernard John V. Tongol[1,2,3]*

[1]Department of Chemistry, College of Science, [2]Research Center for the Natural and Applied Sciences, & [3]Graduate School, University of Santo Tomas, 1015 Manila, Philippines

Direct ethanol fuel cell can serve as alternative to fossil fuels because it is renewable and environmentally-friendly with a high energy conversion efficiency and low pollutant emission. In line with this, an effective anode electrocatalyst should be present which will facilitate the oxidation of the fuel (e.g. ethanol). This study aims to synthesize and characterize a graphene-supported Pd/Ni/Sn electrocatalyst for ethanol oxidation. Modified Hummer's method was used to produce graphene oxide. The Pd/Ni/Sn supported on reduced graphene oxide (RGO) was synthesized using borohydride-facilitated reduction method. Optimization of the product showed that 12 h of reduction time as well as sequential addition of Sn, Ni, and then Pd to the RGO support with atomic ratio kept at 3:2:2 (Pd, Ni, and Sn, respectively) generated the highest maximum current density of 12.64 $mA \cdot cm^{-2}$ at a scan rate of 50 $mV \cdot s^{-1}$. AFM analysis of the synthesized graphene as well as the Pd/Ni/Sn/RGO catalyst composite indicated graphene-like structures having a thickness of 6–8 nm as well as bright particles that could be indicative of metallic particles with an average particle size of 30–40 nm. The synthesized Pd/Ni/Sn/RGO electrocatalyst proved to be effective in facilitating ethanol oxidation in alkaline medium.

Keywords: direct ethanol fuel cell, graphene oxide, Pd/Ni/Sn/RGO electrocatalyst, ethanol oxidation

Introduction

Fossil fuels are the current primary source of energy worldwide. But due to its production of pollutants and waste, there has been a high demand for alternative energy sources. Fuel cells offer a promising alternative as a high performance energy converter and storage device [1]. Fuel cells are known for their many advantages. They are clean and environment-friendly energy source, have high energy conversion efficiency, has low pollutant emission, and has low operating temperature [2].

There are many types of fuel cells including polymer electrolyte membrane fuel cells (PEMFCs) and direct alcohol fuel cells (DAFCs). DAFCs have been gaining a lot of attention due to their portability and easy handling, storage and transport [3]. Methanol as a fuel has been the focus of many studies for its application to DAFCs. However, methanol was found to be toxic, being lethal if

**To whom correspondence should be addressed*
bernard.john.tongol@ust.edu.ph / bjvtongol@yahoo.com

ingested even in small quantities [4]. It was also found to have a high risk of CO poisoning and a tendency to have a high crossover rate in fuel cell systems, meaning that it had sluggish kinetics as it pass through the membrane which cause the fuel cell efficiency to decrease [5]. Among other alcohols, ethanol was found to be a better alternative for methanol as a fuel.

Ethanol is non-toxic, renewable, and readily available. It also has higher energy density and lower crossover rate compared with methanol. The only disadvantage with ethanol is that it has a lower fuel efficiency compared to methanol [6]. The use of a good anodic catalyst is needed to make up for the lower efficiency.

Currently, many have focused on platinum or Pt-based anodic catalysts due to its excellent electrocatalytic activity. Recent studies showed that Pt/Sn provided the best electrocatalytic activity for ethanol oxidation [7]. However, the use of Pt-based electrocatalysts meant higher costs due to being expensive. Pt has also been found to have low tolerance to CO poisoning which lessens the efficiency of fuel cells.

As a substitute, palladium can be used. Pd, compared with Pt, can provide the same electrocatalytic activity for a lower price [8]. It was found that Pd in alkaline media provided better electrocatalytic activity towards ethanol oxidation than that of Pt. Pd is considered as a good alternative to Pt because it is cheaper and also more CO tolerant [9]. Additionally, promoters may also be added to further increase electrocatalytic activity.

Promoters are commonly metals that are added to the main catalyst to improve its activity. Ordinarily, they do not possess any electrocatalytic activity themselves. Known promoters include Ag, Bi, Ni, Sn, Rh, Ru, Ti, and Co. These promoters can increase catalytic activity as well as aid with dispersion of the catalytic material [10]. Many known combinations of Pt and Pd mixed with promoters include Pt-W/C [11], Pd-Co/C [12], Pd-Ni/C [13], Pt-Ir-Sn/C [14], and Pt-Ru-Mo/C [15]. There has been little known study for Pd-based ternary electrocatalysts since majority are focused on Pt-based binary and ternary electrocatalysts.

Graphene is a carbon support that has been gaining much attention since its discovery. Graphene is a monolayer of sp2-bonded carbon atoms tightly packed into a two-dimensional honeycomb lattice. It has a higher surface area support capability compared with known carbon supports such as carbon black and carbon nanotubes [16]. Some have studied mono-metallic and binary electrocatalyst with graphene as support but few have done so with ternary electrocatalysts. Recently, we have synthesized PdNi supported on electrochemically exfoliated graphene oxide [17]. The synthesized catalyst composite gave a higher electrocatalytic performance compared to PdNi supported on carbon black.

Because the performance of fuel cells depends on its components and material make-up, it is therefore needed to carefully study the electrocatalysts employed as well as its performance for the improvement of the fuel cell [18]. The research aims to identify the effect of applying a ternary electrocatalyst consisting of Pd/Ni/Sn supported on graphene for the oxidation of ethanol in direct ethanol fuel cells.

Experimental

Materials and reagents. Graphite powder (Showa Chemical Industry Ltd.) was used as the graphene source. $NaNO_3$ (Merck), concentrated H_2SO_4 (RCI Labscan), $KMnO_4$ (Scharlau), and 30% H_2O_2 (Sigma-Aldrich) were used following modified Hummer's method. $PdCl_2$ (Sigma-Aldrich), $SnCl_2$ (Sigma-

Aldrich), and $NiCl_2$ (Sigma-Aldrich) were used as metal sources. Each metal salt was diluted to 10 mM; $PdCl_2$ was dissolved using KBr (Merck), $SnCl_2$ was dissolved using 1M HCl (J. T. Baker), and ultrapure H_2O obtained from Direct Q UV 3 (Millipore Co., USA) was used for $NiCl_2$. $NaBH_4$ (Sigma-Aldrich) was used for the reduction reaction step. Purification and drying were done using Operon Freeze Dryer. Absolute EtOH (J. T. Baker) diluted to 1.0 M using 0.1 M NaOH (RCI Labscan) was used as medium for the electrochemical analysis. DMF (RCI Labscan) and 5% Nafion® (Sigma-Aldrich) were used for the preparation of the catalyst ink.

Synthesis of graphene oxide. The synthesis of graphene oxide was based on modified Hummer's method. Graphite powder (3.0 g) was grinded and transferred to a 1-L Erlenmeyer flask. $NaNO_3$ (1.5 g) and concentrated H_2SO_4 (125 mL) was then added. The solution was then stirred in an ice bath for 10 minutes (time starts when 10°C was reached). $KMnO_4$ (9.0 g) was then slowly added while keeping the temperature from exceeding 30°C. The solution was then warmed at 35°C with stirring for 30 min. Ultrapure H_2O (150 mL) was then added slowly and carefully. The solution was then heated at 98°C for 15 min. A solution of 30% H_2O_2 (10 mL) was then added and the resulting solution was then freeze-dried.

Synthesis of Pd/Ni/Sn/RGO composite. Solutions containing the Pd, Ni, and Sn metals were initially prepared. A mass 40 mg of the synthesized graphene oxide was transferred to a 250 mL Erlenmeyer flask. Ultrapure H_2O (100 mL) was added, then the solution was subjected to ultrasonication until the particles were fully dispersed. The appropriate amount of the metal solution was then added. The pH of the solution was then adjusted to 10 using 1.0 M NaOH. $NaBH_4$ (400 mg) was then added in the solution. The solution was then stirred for 12 h until reduction reaction is complete. The solution was then filtered and washed until chloride was removed (checked using $AgNO_3$ indicator). The residue was then transferred to a vial and was freeze-dried. The resulting Pd/Ni/Sn on reduced graphene oxide (RGO) composite was then treated for characterization.

Characterization. All electrochemical measurements were done in a 3-electrode electrochemical cell at room temperature. A Pt counter electrode and Ag/AgCl (sat. 3 M KCl) reference electrode was used. All electrochemical measurements were carried out using a potentiostat (EDAQ, Australia). The resulting Pd/Ni/Sn/RGO composite (1mg) was transferred in a small vial. Nafion® (0.04 mL) and DMF (0.96 mL) were then added. The mixture was then subjected to sonication for 1 h to form the catalyst ink. Around 2 mL of the ink was drop casted on a glassy carbon electrode (GCE) and was oven dried for 15 min (80°C). The potential range of –900 mV to 400 mV (vs. Ag/AgCl) with a scan rate of 50 $mV \times s^{-1}$ for 25 cycles were used throughout the study.

The surface morphology of the prepared electrocatalyst was investigated using a non-contact atomic force microscope (Park Systems NX10). A PPP-NCHR tip with a tip radius of curvature of 10 nm, nominal frequency of 330 kHz, and a force constant of 43 $N \cdot m^{-1}$ was used to probe the samples. The catalyst ink was prepared by transferring 1 mg of the metal/RGO composite to a small vial. DMF (1 mL) was then added and the mixture was subjected to sonication for 1 h. The catalyst ink was then drop casted on a GCE and was oven dried for about half a day (80°C).

Results and discussion

Characterization of electrocatalytic activity using cyclic voltammetry

Optimization of reduction time. The time needed for complete deposition of the metal particles to the carbon support is dictated by the duration of the reduction reaction needed for the said process. Sodium borohydride reduction method entails the addition of $NaBH_4$ to a reaction flask containing the Pd metal and carbon support under constant stirring for a certain period of time. For this optimization, 20% metal loading was maintained for all prepared electrocatalyst. A synthesized Pd/RGO electrocatalyst was used for this optimization for convenience since it will give a clear CV profile. Figure 1 shows the CV profiles that were collected while Table 1 shows a summary of the results.

The results show that the Pd/RGO reduced for 12h generated the highest maximum current density compared with the other two samples. From here, the optimized reduction time was set at 12 h.

Optimization of metal loading sequence. The next optimization done was on the sequence of deposition of the metals to the graphene support. Again, 20% metal loading was maintained for all prepared electrocatalysts. The atomic ratio between the metals was set at 1:1:1. Figure 2 shows that the Pd/NiSn/RGO electrocatalyst (Pd was added last while Ni and Sn were added together) gave a higher current density of 2.03 $mA \cdot cm^{-2}$ compared to that of NiSn/Pd/RGO. With this information, the sequence between Ni and Sn was modified while Pd was kept at being added last. Based on the CV profiles from Fig. 2 and Fig. 3, the

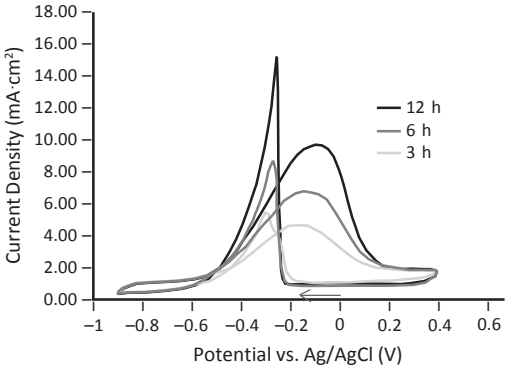

Figure 1. CV profiles of samples at various reduction time of Pd/RGO in 1.0 M ethanol in 0.1 M NaOH (50 $mV \cdot s^{-1}$, 25th cycle)

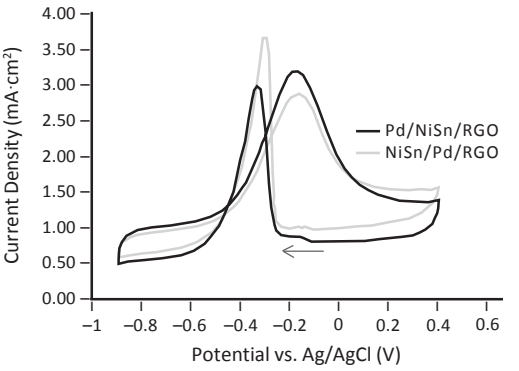

Figure 2. CV profiles of NiSn/Pd/RGO and Pd/NiSn/RGO in 1.0 M ethanol in 0.1 M NaOH (50 $mV \cdot s^{-1}$, 25th cycle)

Table 1. Comparison between Pd/RGO samples reduced for 3 h, 6 h, and 12 h

Catalyst	Onset Potential (V)	Peak Potential (V)	Maximum Current Density ($mA \cdot cm^{-2}$)	Repeatability (n=3)
3 h Sample	–0.672	–0.264	4.63	%RSD=10.21%
6 h Sample	–0.667	–0.148	6.69	%RSD=30.82%
12 h Sample	–0.663	–0.092	9.72	%RSD=6.53%

Table 2. Comparison between samples of differing metal loading sequences

Catalyst	Onset Potential (V)	Peak Potential (V)	Maximum Current Density ($mA \cdot cm^{-2}$)	Repeatability (n=3)
Pd/Ni/Sn/RGO	–0.529	–0.114	4.56	%RSD=13.03
Pd/Sn/Ni/RGO	–0.481	–0.104	1.12	%RSD=11.36
Pd/NiSn/RGO	–0.661	–0.185	2.03	%RSD=9.06
NiSn/Pd/RGO	–0.619	–0.173	1.62	%RSD=7.24

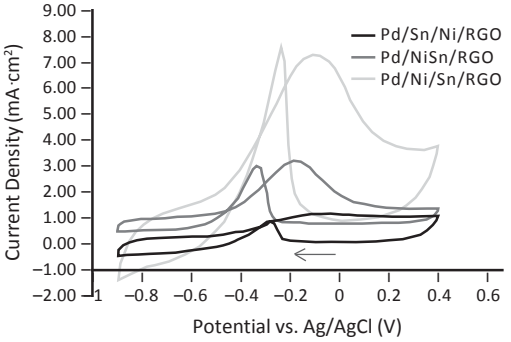

Figure 3. CV profiles of Pd/Ni/Sn/RGO, Pd/Sn/Ni/RGO, and Pd/NiSn/RGO in 1.0 M ethanol in 0.1 M NaOH ($50 mV \cdot s^{-1}$, 25th cycle)

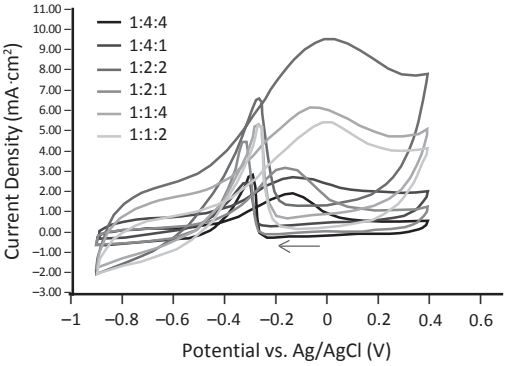

Figure 4. CV profiles of Pd/Ni/Sn/RGO composites with ratios of 1:2:1, 1:4:1, 1:1:2, 1:1:4, 1:2:2, and 1:4:4 in 1.0 M ethanol in 0.1 M NaOH ($50 mV \cdot s^{-1}$, 25th cycle)

Pd/Ni/Sn/RGO sample proved to be better compared to the other three. This shows that adding the promoters first enhanced the electrocatalytic activity of the ternary system. It could be that adding Sn first and then Ni promoted the active sites of the main catalyst Pd [19]. Table 2 presents a summary of the CV characteristics.

Results show that the Pd/Ni/Sn/RGO electrocatalyst gave the highest maximum current density of 4.56 $mA \cdot cm^{-2}$ among the other samples. The sequential addition of Sn, Ni, and then Pd to the RGO carbon support was used all throughout the next steps of optimization.

Optimization of atomic ratio. The next to be optimized was the atomic ratio of the metals deposited on RGO. Samples of varying atomic ratios were prepared and subjected to cyclic voltammetry. A metal loading of 20% was maintained. The first part of this optimization focused on altering the ratio between Ni and Sn. From Fig. 4, the ratio of 1:2:2 for Pd, Ni, and Sn respectively gave the highest maximum current density among the other combinations. Setting the ratio of Ni and Sn as 2:2, the atomic ratio for Pd was then modified for a different set of samples and Fig. 5 shows that the ratio of 3:2:2 for Pd, Ni, and Sn respectively gave the highest maximum current density among the rest. Table 3 summarizes the CV characteristics from Fig. 4 and Fig. 5.

The sample with the ratio of 3:2:2 generated the highest maximum current density of 12.64 $mA \cdot cm^{-2}$.

Comparison of Pd/Ni/Sn/RGO with mono-metallic and binary electrocatalysts. Other electrocatalysts were synthesized for

Table 3. Comparison between Pd/Ni/Sn/RGO composites with differing atomic ratios

Ratio (Pd/Ni/Sn)	Onset Potential (V)	Peak Potential (V)	Maximum Current Density ($mA \cdot cm^{-2}$)	Repeatability (n=3)
1:2:1	–0.564	–0.161	2.46	%RSD=10.05
1:4:1	–0.549	–0.135	1.32	%RSD=7.95
1:1:2	–0.504	–0.021	2.61	%RSD=9.24
1:1:4	–0.495	–0.071	2.62	%RSD=14.61
1:2:2	–0.573	–0.038	3.81	%RSD=16.53
1:4:4	–0.451	–0.136	1.52	%RSD=3.53
1:2:2	–0.573	–0.038	3.81	%RSD=16.53
2:2:2	–0.529	–0.114	4.56	%RSD=10.21
3:2:2	–0.610	–0.048	12.64	%RSD=9.01
4:2:2	–0.605	–0.082	7.22	%RSD=29.31
5:2:2	–0.578	–0.075	6.01	%RSD=5.05
6:2:2	–0.530	–0.058	3.46	%RSD=12.76

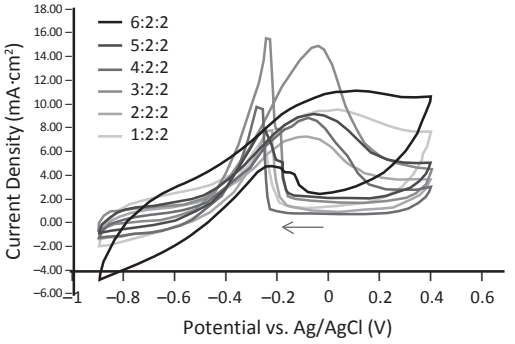

Figure 5. CV profiles of Pd/Ni/Sn/RGO composites with ratios of 1:2:2, 2:2:2, 3:2:2, 4:2:2, 5:2:2, and 6:2:2 in 1.0 M ethanol in 0.1 M NaOH (25th cycle)

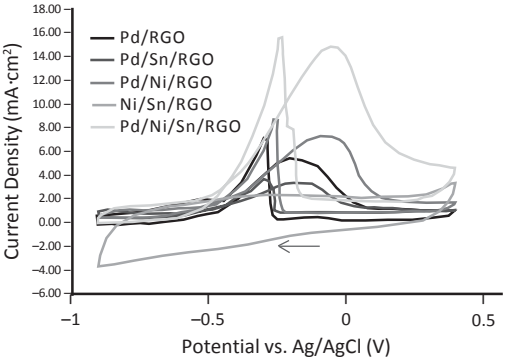

Figure 6. CV profiles of Pd/RGO, Pd/Sn/RGO, Pd/Ni/RGO, Ni/Sn/RGO, and Pd/Ni/Sn/RGO composites in 1 M ethanol in 0.1 M NaOH ($50 mV \cdot s^{-2}$, 25th cycle)

comparative purposes. Pd/RGO, Pd/Ni/RGO, Pd/Sn/RGO, and Ni/Sn/RGO electrocatalysts were subjected to CV and results were compared with the final Pd/Ni/Sn/RGO electrocatalyst. From Fig. 6, the Ni/Sn/RGO composite gave no electrocatalytic activity toward ethanol oxidation. The binary catalyst Pd/Sn/RGO gave a higher current density than that of the Pd/RGO and Pd/Ni/RGO. In some systems, it was found out that Ni can modify the electronic structure of the main catalyst which lessens adsorbed CO and allows better ethanol oxidation performance [20]. The ternary catalyst was found to give a higher current density than the mono-metallic and binary catalysts. The addition of two promoters to the main Pd catalyst was able to improve the generated current density significantly. The promoters served as shielding for the main catalyst and also blocked inactive sites causing an increase in reaction rate which lead to the improved electrocatalytic activity [19].

Characterization of surface morphology using atomic force microscopy

AFM analysis of graphene. Non-contact atomic force microscopy (nc-AFM) constructs images through force interactions between the

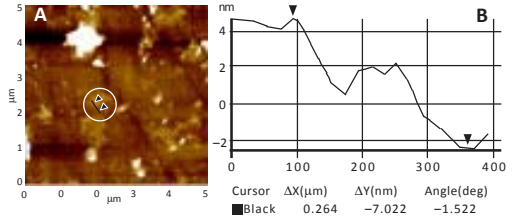

Figure 7. A) AFM image of RGO and B) height sample readings

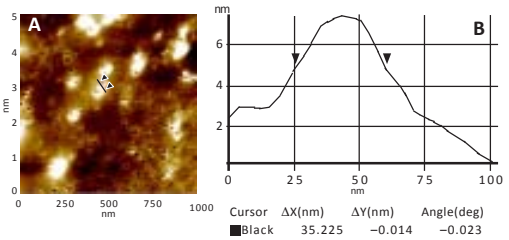

Figure 8. A) AFM image of Pd/Ni/Sn/RGO composite on GCE substrate and B) height particle analysis

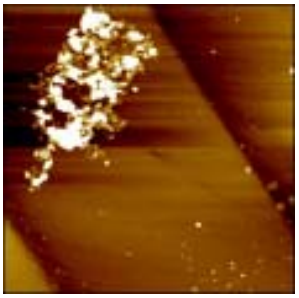

Figure 9. AFM image of Pd/Ni/Sn/RGO (1000×1000 nm) (arrows point towards possible graphene structures)

probe and sample [21]. Synthesized graphene oxide was reduced using $NaBH_4$. The resulting reduced graphene oxide (RGO) was dissolved in DMF, drop casted on a glassy carbon electrode (GCE), and was analyzed using AFM. AFM images of RGO were recorded and presented in Fig. 7.

From the results of the AFM, graphene-like structures were observed on the surface of GCE substrate. The graphene-like structures exhibited a height of around 6–8 nm. Theoretically, graphene should sustain a two-dimensional form and have a thickness ranging from 0.35 nm to 1 nm. However, certain parameters such as sample preparation, laboratory conditions, and measurement conditions would cause anomalies to arise in measuring the thickness of synthesized graphene [22]. Still, the measured thickness of 6–8 nm is still acceptable and can be classified as graphene-like since it has been studied that graphene can have a thickness of 10 nm and below, with 1 nm per layer of graphene [23]. It can therefore be said that the synthesis of graphene through reduction of GO was successful.

AFM analysis of Pd/Ni/Sn/RGO. The optimized Pd/Ni/Sn/RGO composite was also prepared and investigated using AFM. The AFM images were recorded and the particles size was analyzed as presented in Fig. 8.

Figure 8 shows bright particles that could be attributed to the metallic particles. The Pd/Ni/Sn particles show an average lateral dimension of 30–40 nm. The small black holes that can be seen in the AFM image (Fig. 8) are likely to be surface defects that arose during the drying process. Figure 9 shows that there is interaction between the metal particles and the graphene support where arrows point towards possible graphene structures.

Figure 9 shows interaction between the Pd/Ni/Sn particles and the RGO support. The arrows show near see-through clusters which are likely graphene. The bright particles are the Pd/Ni/Sn metal particles on the surface of graphene. Overall, the image indicates that RGO indeed acted as carbon support for the synthesized ternary electrocatalyst.

Conclusion

A Pd/Ni/Sn/RGO electrocatalyst was successfully synthesized and characterized using cyclic voltammetry and atomic force microscopy. Modified Hummer's method was effective in synthesizing graphene oxide. $NaBH_4$ reduction of the synthesized GO together with the metal solution was able to produce the desired ternary catalyst. Through different optimizations done using CV, it was found out that a reduction time of 12 h and sequential addition of Sn, Ni, and then Pd with an atomic ratio of 3:2:2 for Pd, Ni, and Sn, respectively, gave a good maximum current density of 12.64 $mA \cdot cm^{-2}$. Comparing this result with mono-metallic and binary electrocatalyst (Pd/RGO, Pd/Ni/RGO, Pd/Sn/RGO, and Ni/Sn/RGO) showed that the prepared ternary electrocatalyst gave the best performance. Analysis of morphology using AFM showed that the synthesized reduced graphene oxide had an average thickness of 6–8 nm indicating six to eight layers of graphene. AFM analysis of the Pd/Ni/Sn particles showed an average lateral dimension of 30–40 nm and that there is interaction between the metallic particles and the RGO carbon support.

Overall, the addition of Ni and Sn forming the Pd/Ni/Sn/RGO electrocatalyst had shown enhanced performance in facilitating ethanol oxidation in an alkaline medium system.

Acknowledgment

The research funding from the Philippine Council for Industry, Energy, and Emerging Technology Research and Development of the Department of Science and Technology (PCIEERD-DOST) is gratefully acknowledged.

References

[1] Kung C, Lin P, Xue Y, Akolkar R, Dai L, Yu X, & Liu C. Three dimensional graphene foam supported platinum–ruthenium bimetallic nanocatalysts for direct methanol and direct ethanol fuel cell applications. *J. Power Sources* **2014**; 256:329–335.

[2] Zhang Y, Shu H, Chang G, Ji K, Oyama M, Liu X, & He Y. Facile synthesis of palladium–graphene nanocomposites and their catalysis for electro-oxidation of methanol and ethanol. *Electrochim. Acta* **2013**; 109:570–576.

[3] An H, Pan L, Cui H, Li B, Zhou D, Zhai J, & Li Q. Synthesis and performance of palladium-based catalysts for methanol and ethanol oxidation in alkaline fuel cells. *Electrochim. Acta* **2013**; 102:79–87.

[4] Klein D. *Organic Chemistry* (1st Edition). (Hoboken, N.J.: John Wiley & Sons, Inc., **2012**).

[5] Neto AO, Dias RR, Tusi MM, Linardi M, & Spinacé EV. Electro-oxidation of methanol and ethanol using PtRu/C, PtSn/C and PtSnRu/C electrocatalysts prepared by an alcohol-reduction process. *J. Power Sources* **2007**; 166(1):87–91.

[6] Pereira JP, Falcão DS, Oliveira VB, & Pinto AMFR. Performance of a passive direct ethanol fuel cell. *J. Power Sources* **2014**; 256:14–19.

[7] Kamarudin MZF, Kamarudin SK, Masdar MS, & Daud WRW. Review: Direct ethanol fuel cells. *Int. J. Hydrogen Energ.* **2012**; 38(22):9438–9453.

[8] Awasthi R & Singh RN. Graphene-supported Pd–Ru nanoparticles with superior methanol electrooxidation activity. *Carbon* **2013**; 51:282–289.

[9] Liang ZX, Zhao TS, Xu JB, & Zhu LD. Mechanism study of the ethanol oxidation reaction on palladium in alkaline media. *Electrochim. Acta* **2009**; 54(8):2203–2208.

[10] Keresszegi C. On the Mechanism of the Aerobic Oxidation and Dehydrogenation of Alcohols on Palladium and Platinum. Retrieved from ETH E-Collection. (Diss. ETH No 16008), **2005**.

[11] Zhou WJ, Li WZ, Song SQ, Zhou ZH, Jiang LH, Sun GQ, … & Tsiakaras P. Bi- and tri-metallic Pt-based anode catalysts for direct ethanol fuel cells. *J. Power Sources* **2004**;131(1–2):217–223.

[12] Wang W, Zheng D, Du C, Zou Z, Zhang X, Xia B, … & Akins DL. Carbon-supported Pd-Co bimetallic nanoparticles as electrocatalysts for the oxygen reduction reaction. *J. Power Sources* **2007**; 167(2):243–249.

[13] Zhang Z, Xin L, Sun K, & Li W. Pd–Ni electrocatalysts for efficient ethanol oxidation reaction in alkaline electrolyte. *Int. J. Hydrogen Energ.* **2011**; 36(20):12686–12697.

[14] Tayal J, Rawat B, & Basu S. Bi-metallic and tri-metallic Pt–Sn/C, Pt–Ir/C, Pt–Ir–Sn/C catalysts for electro-oxidation of ethanol in direct ethanol fuel cell. *Int. J. Hydrogen Energ.* **2011**; 36(22):14884–14897.

[15] Martínez-Huerta MV, Tsiouvaras N, García G, Peña MA, Pastor E, Rodriguez JL, & Fierro JG. Carbon-Supported PtRuMo Electrocatalysts for Direct Alcohol Fuel Cells. *Catalysts (2073-4344)* **2013**; 3(4):811–838.

[16] Singh V, Joung D, Zhai L, Das S, Khondaker SI, & Seal S. Graphene based materials: Past, present and future. *Prog. Mater. Sci.* **2011**; 56(8):1178–1271.

[17] Tan JL, Villar PG, de Jesus A, & Tongol BJV. A green approach to the synthesis of Pd-Ni/Graphene via electrochemical exfoliation of graphite from used battery for the electrocatalysis of ethanol. *J. Chinese Chem. Soc.* **2014**; 61(7):774–777.

[18] Beyhan S, Coutanceau C, Léger J, Napporn TW, & Kadýrgan F. Promising anode candidates for direct ethanol fuel cell: Carbon supported PtSn-based trimetallic catalysts prepared by Bönnemann method. *Int. J. Hydrogen Energ.* **2013**; 38(16):6830–6841.

[19] Keresszegi C, Mallat T, Grunwaldt J, & Baiker A. A simple discrimination of the promoter effect in alcohol oxidation and dehydrogenation over platinum and palladium. *J. Catal.* **2004**; 225(1):138–146.

[20] Parreira LS, da Silva JCM, Silva MD, Simões FC, Garcia S, Gaubeur I, … & dos Santos MC. PtSnNi/C nanoparticle electrocatalysts for the ethanol oxidation reaction: Ni stability study. *Electrochim. Acta* **2013**; 96:243–252.

[21] Binnig G, Quate CF, & Gerber C. Atomic Force Microscope. *Phys. Rev. Lett.* **1986**; 56(9):930–933.

[22] Nemes-Incze P, Osváth Z, Kamarás K, & Biró LP. Anomalies in thickness measurements of graphene and few layer graphite crystals by tapping mode atomic force microscopy. *Carbon* **2008**; 46(11):1435–1442.

[23] Geim AK & Novoselov KS. The rise of graphene. *Nature Materials* **2007**; 6(3):183–91.